

SMOS Freeze and Thaw Processing and Dissemination Service

Algorithm Theoretical Baseline Document

ESRIN Contract Nro: 4000124500/18/I-EF

Issue / Revision: 3 / 4

Date: 16 October 2023

Prepared by

Kimmo Rautiainen, Manu Holmberg
Finnish Meteorological Institute (FMI)



ILMATIETEEN LAITOS
METEOROLOGISKA INSTITUTET
FINNISH METEOROLOGICAL INSTITUTE

This page is intentionally left blank.

Document change log

Issue/ Revision	Date	Observations
1.0	22-Dec-2015	First issue
1.1	18-Aug-2016	Updated version
2.0	13-Nov-2018	First version for SMOS Freeze and Thaw Processing and Dissemination Service
2.1	26-Nov-2018	Table 1 and Figure 3 updated
2.2	28-Feb-2019	Table 1: soil state values updated + minor updates
3.0	21-Oct-2021	Updated version for F/T processor 3.00
3.1	07-Jun-2023	Updates in section 3.2
3.2	25-Jul-2023	Updates based on ESA comments
3.3	19-Sep-2023	Section 3.2 (page 8 and Figure 3) updated
3.4	16-Oct-2023	Section 2.2 updated

This page is intentionally left blank.

Contents

1	Introduction	5
2	Input data	6
2.1	SMOS data	6
2.2	Ancillary data	6
3	Algorithm description	7
3.1	Physical basis	7
3.2	Implementation	8
3.2.1	Converting CATDS SMOS L3TB data to MATLAB	9
3.2.2	Data quality filtering	10
3.2.3	Noise removal and generation of daily files with Kalman filter	11
3.2.4	Frozen and thaw ground references	13
3.2.5	Initial classification and error estimate	14
3.2.6	Processing mask	15
3.2.7	Soil state product generation	16
4	References	18

1 Introduction

This document presents the soil freeze and thaw state detection algorithm originally developed within the SMOS+ Innovation Permafrost (ESA ESRIN Contract no: 4000105184/12/I-BG) project and development continued within SMOS+ Frost2Study (ESRIN Contract no: 4000110973/14/NL/FF/lf). The latest version of the algorithm has been finalised within SMOS Freeze and Thaw Processing and Dissemination Service contract (ESRIN Contract no: 4000124500/18/I-EF).

The soil freeze/thaw state algorithm uses a threshold detection approach to determine the average soil state of each SMOS observation grid cell. Reference signatures for frozen and thawed states are defined for each cell from the historical database of observations. Based on comparisons to these references, soil state is categorized into three states: thawed, partially frozen or frozen. Ancillary data on 2 meters air temperature and snow cover are applied to regulate the detection. The ancillary data are used to (1) automatically determine the periods during which the frozen and thaw references can be defined, and to (2) remove obvious errors from the product output.

The soil state detection algorithm uses as input data CATDS (Centre Aval de Traitement des Données SMOS) Level 3 polar gridded brightness temperatures from incidence angle range from 50 degrees to 55 degrees.

The theoretical basis of the algorithm has been published in several journal articles (Rautiainen et al., 2012; Rautiainen et al., 2014; Rautiainen et al., 2016)

2 Input data

2.1 SMOS data

The L3FT algorithm uses CATDS (Centre Aval de Traitement des Données SMOS) Level 3 brightness temperature product (L3TB). Current CATDS L3TB processor version is 331, which correspond to the level 1 SMOS DPGS version v724. The L3TB data is in ground polarization frame $p = v, h$ and provided in the Equal-Area Scalable Earth Grid (EASE 2.0) in polar projection (720×720 pixels). Daily files include all swaths observed over the Northern hemisphere. The brightness temperatures are provided as average values in incident angle bins with 5-degree intervals. The L3TB product files are in NetCDF format.

2.2 Ancillary data

Two ancillary datasets are used by the L3FT algorithm, (1) daily average 2m air temperature data, and (2) daily snow cover data. The daily 2 meter air temperature data is downloaded from the ECMWF database. ERA5-Land surface layer air temperature data (Muñoz Sabater, J., 2019) is used for period from June 1st 2010 to October 10th 2023. For operational use near real time (NRT) data is required, SMOS FT uses IFS forecast data, as default it is available when new CATDS L3 dataset is generated. ERA5-Land data are gridded at a spatial resolution of $0.1^\circ \times 0.1^\circ$, and IFS forecast data at a spatial resolution of $0.25^\circ \times 0.25^\circ$. For both datasets the daily temperature information is given in 6 hour intervals at 00, 06, 12, and 18 hours. In SMOS FT processor, daily average is calculated from the input data, and data are re-projected to EASE-2 grid (polar projection) and resampled to $25 \text{ km} \times 25 \text{ km}$ spatial resolution. The daily snow cover data consists of the National Oceanic and Atmospheric Administration's (NOAA) / National Environmental Satellite and Information Service (NESDIS) data from the Interactive Multi-sensor Snow and Ice Mapping System, IMS. The IMS dataset provides daily information on snow cover (Helfrich et al, 2007). Input spatial resolution of 4 km is used. In SMOS FT processor, data are re-projected to EASE-2 grid (polar projection) and resampled to $25 \text{ km} \times 25 \text{ km}$ spatial resolution.

3 Algorithm description

3.1 Physical basis

The physical basis of soil F/T detection at passive microwave observations is based on the difference in emissivity between frozen and thaw soil. The presence of free liquid water in thaw soils increases the effective dielectric constant compared to frozen soil, thus decreasing emissivity and brightness temperature. On the other hand, freezing of the liquid soil water-phase affects the detected microwave emission in the same way as drying of the soil does, i.e. emissivity is increased. Figure 1 shows the calculated spectra of the real and imaginary parts of the complex dielectric constant $\epsilon = \epsilon' + i \cdot \epsilon''$ for pure ice and pure water (Mätzler et. al 2006). For liquid water, the real part of the relative dielectric constant is close to $\epsilon' \approx 90$ at L-band; for fast pure ice it is $\epsilon' \approx 3.2$ across the microwave range. For higher microwave frequencies, ϵ' of free water is increasingly closer to that of ice, as a consequence of relaxation at $f_r \approx 8\text{GHz}$, thus decreasing the potential contrast in emissivity between water and, for example, moist soils in frozen or unfrozen states. Changes in

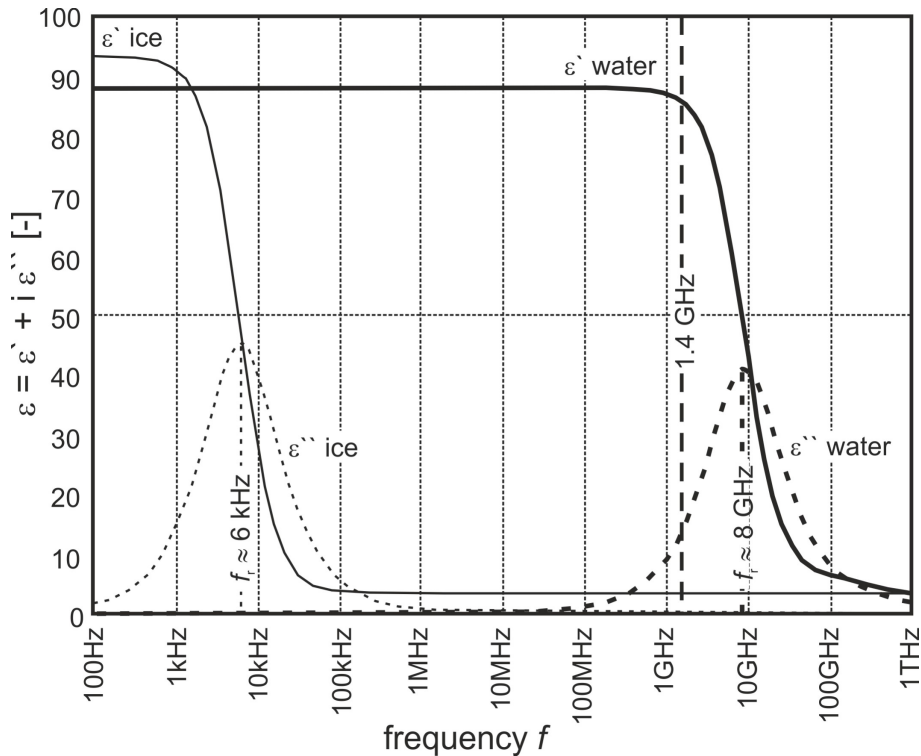


Figure 1: Spectra of the complex relative dielectric constant of pure ice at $T = 270$ K and pure water at 273 K. Real parts are shown as solid lines and imaginary parts as dashed lines. At L-band (1.4 GHz) the permittivity contrast between the liquid water and ice is very large (figure from Rautiainen et al. 2014)

the permittivity of soil affect the measured brightness temperatures. The lower the permittivity of the target is, the higher emissivity it has. Following from the Fresnel equations the change of a dielectric contrast between two media will affect the two linear polarizations, horizontal and vertical, differently at incidence angles greater

than zero. The power difference of emitted signals between vertical and horizontal polarizations can be expected to be smaller for frozen soil than for unfrozen soil. As a result, the polarization difference $T_B^V - T_B^H$ is decreased for frozen soil compared to thaw soil situation. The core of the algorithm is based on calculating the normalized polarization ratio (NPR) for each observation.

$$NPR \stackrel{\text{def}}{=} \frac{T_B^V - T_B^H}{T_B^V + T_B^H}, \quad (1)$$

One advantage of the NPR is the inherent insensitivity to physical temperature; which would be required for the direct observation of brightness temperature

3.2 Implementation

The practical implementation of the algorithm is described in this section. The main script of the processing software is written in MATLAB. All the re-projection routines are made with GDAL GIS software. GDAL commands use also some Python code extensions. Generation of quicklook images uses SAGA GIS routines.

The SMOS Freeze and Thaw processing service consists of two separate SMOS FT processors: the operational FT processor and the re-processing FT processor. The re-processing processor is used when all existing input data is processed in one processor run. The operational processor generates the daily soil FT output products. There are two differences between the processors: (1) The re-processing processor uses ECMWF ERA5-Land data and the operational processor uses ECMWF IFS forecast data for the 2-metre air temperature data source. (2) The frozen and thaw ground references are generated with the re-processing processor when all existing data are processed. These references are used with the operational processor. The high level flowchart of the re-processing FT processor and the operational FT processor are shown in Figures 2 and 3, respectively.

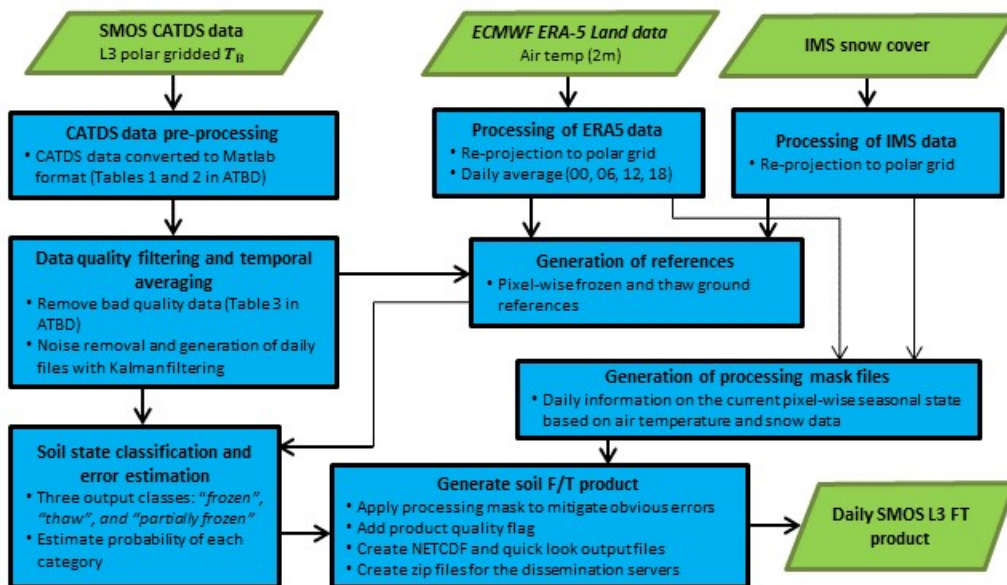


Figure 2: The high level flowchart of the re-processing FT processor.

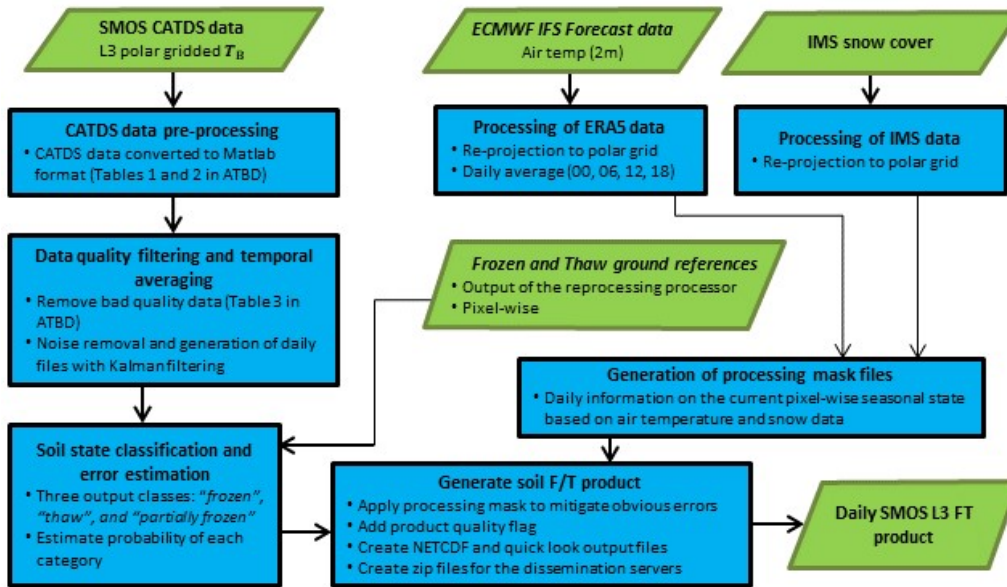


Figure 3: The high level flowchart of the operational FT processor.

3.2.1 Converting CATDS SMOS L3TB data to MATLAB

CATDS SMOS L3TB data file contain measurements from a single swath. The data fields that are used from the L3TB data file are summarized in the table 1. For the use of L3FT algorithm, the normalized polarization value is computed and saved with other relevant data fields into a MATLAB data file. Table 2 summarizes the structure of MATLAB data file.

Description	CATDS L3TB field names	Unit
H and V polarized Brightness temperatures	BT_H, BT_V	K
Standard deviations of the H and V polarized Brightness temperatures	Pixel_BT_Standard_Deviation_H, Pixel_BT_Standard_Deviation_V	K
Radiometric accuracies at H and V polarizations	Pixel_Radiometric_Accuracy_H, Pixel_Radiometric_Accuracy_V	K
Number of views	Nviews	1
Number of views suspected to be affected by RFI	Nb_RFI_Flags	1
Number of views suspected to be affected by the Sun	Nb_SUN_Flags	1
Grid point latitude and longitude information	latitude, longitude	deg
Day of the observation from 01-Jan-2000	Days	1
Second of the observation	UTC_Seconds	s

Table 1: Relevnant CATDS SMOS L3TB data fields used by the L3FT processor.

Description	Field name	Type
Incident angle	ang	double
Incident angle bin	ang_ind	int
Brightness temperature inside physical bounds flag	btp_physical	flag
χ^2 values from H and V polarizations	chi2_min, chi2_max	double
observation time	dnum	double
Normalized polarization ratio	npr	double
Normalized polarization ratio variance	npr_var	double
Orbit	orb	int
Number of views suspected with RFI contamination	rfi	int
Number of views suspected with SUN contamination	rfi	int
Number of views	views	int

Table 2: Content of single swath file in the L3FT processor.

3.2.2 Data quality filtering

Before applying temporal filtering, measurements with decreased quality are filtered out. Table 3 summarizes the quality filtering criteria. First, the brightness temperature values are expected to be within expected range. In freeze-thaw detection framework, values larger than 300K can be omitted. Second, its required that the incident angle bin contains at least 5 measurements to have reliable average value. Third, the ratio between sample standard deviation of measurements and radiometric accuracy in the incident angle bin

$$\chi = \frac{T_B \text{ deviation}}{T_B \text{ accuracy}} \quad (2)$$

is expected to be bounded. Fourth, the fraction of RFI contaminated measurements within the incident angle bin is required to be less than 40%.

Description	Criteria
Realistic brightness temperature values	$0 \leq T_B^{V,H} \leq 300$
Sufficient amount of views within the incident angle bin	$5 \leq N_{\text{views}}$
Realistic sample deviation compared to radiometric accuracy	$0.1 \leq \chi \leq 2$
Low RFI contamination	$N_{\text{RFI}}/N_{\text{views}} \leq 40\%$

Table 3: Data filtering criteria in the SMOS L3FT processor.

3.2.3 Noise removal and generation of daily files with Kalman filter

Temporal filtering is applied to the swath files to (1) remove noise from the signal, and (2) to generate daily files with full coverage of the globe. The temporal filtering is done for each grid point independently. This section describes the Kalman filter algorithm which is used.

For a fixed grid point, let r_k^* denote the observed normalized polarization ratio value at the time t_k with $k = 1, 2, 3 \dots$ being indexing variable. Since this is computed from brightness temperature measurements containing noise, the signal r_k^* contains noise as well as is related to the true physical polarization ratio value r_k by

$$r_k^* \sim \mathcal{N}(r_k, v_k^2) \quad (3)$$

with variance

$$v_k^2 = \frac{\text{var } T_k^v + \text{var } T_k^h}{(T_k^v + T_k^h)^2}. \quad (4)$$

Above T_k^p denote the observed brightness temperature and $\text{var } T_k^p$ the corresponding variance. To extract information about the unknown physical time series r_k (i.e. to remove noise), the time series is modeled as a linear dynamical system (LDM)

$$\begin{cases} r_k &= r_{k-1} + W_k, \\ r_k^* &= r_k + V_k, \end{cases} \quad (5)$$

where W_k and V_k are random variables with the following normal distributions

$$\begin{cases} W_k &\sim \mathcal{N}(0, \theta^2) \\ V_k &\sim \mathcal{N}(0, v_k^2). \end{cases} \quad (6)$$

The standard deviation v_k is computed from the input data according to equation (4) while the parameter θ is considered a fitting parameter that specifies how fast the signal can change between two consecutive measurements. Estimate for the physical signal r_k , given the noisy measurements r_k^* up to that point in time, is given by the Kalman filter (KF) algorithm. For this simple special case of LDM, the KF algorithm can be written as

$$\begin{cases} r_k &= (1 - a_k)r_{k-1} + a_k r_k^*, \\ u_k^2 &= (1 - a_k)(u_{k-1}^2 + \theta^2), \end{cases} \quad (7)$$

where r_k is the filtered time series and u_k the corresponding standard deviation at the time t_k . The coefficient a_k is a special case of the Kalman gain matrix and is given by

$$a_k = \frac{u_{k-1}^2 + \theta^2}{v_k^2 + u_{k-1}^2 + \theta^2}. \quad (8)$$

In particular, the filtered value r_k is a weighted average of the noisy measurement r_k^* and the previous filtered value r_{k-1} . The weights depend only on the measurement error v_k , uncertainty of the filtered signal in the previous step u_{k-1} , and the fitting parameter θ . Figure 4 shows an example of the filtered time series against noisy

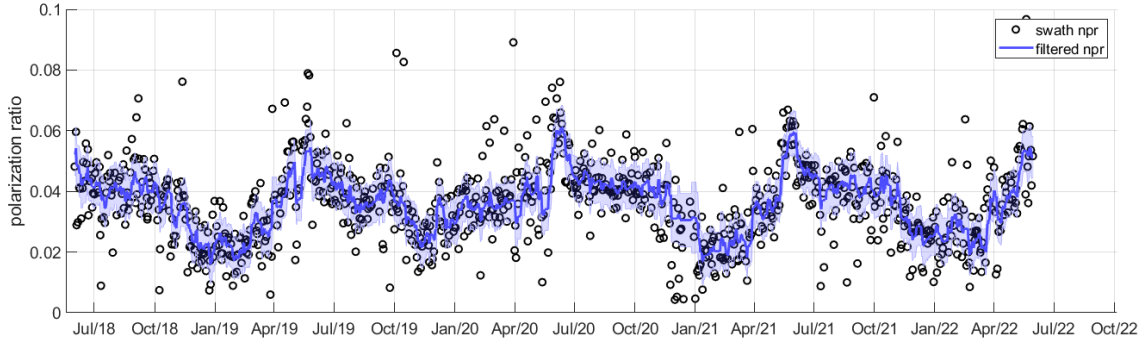


Figure 4: Time series of swath and filtered normalized polarisation ratio from EASE2.0 grid point centered at 67.3693N, 26.9479E

measurements. There is a trade-off in the choice of the parameter θ . On the one hand, high values leave noise to the filtered signal but on the other hand low values introduce lag into the filtered series, i.e. time series becomes less responsive to actual physical changes. To balance between these two effects, the choice of the parameter θ is important. The parameter θ can be fitted to the measurements by maximizing likelihood of the linear dynamical model (3.2.3). The likelihood is given by

$$p(r_1^*, \dots, r_N^* | \theta) = p(r_1^*) \prod_{k=2}^N p(r_k^* | r_1^*, \dots, r_{k-1}^*, \theta), \quad (9)$$

where the components of the product are given by

$$p(r_k^* | r_1^*, \dots, r_{k-1}^*, \theta) = \frac{1}{\sqrt{2\pi}u_{k-1}} \exp\left(-\frac{(r_k^* - r_{k-1}^*)^2}{2u_{k-1}^2}\right). \quad (10)$$

These are computed simultaneously at each iteration of the algorithm (7), thus providing the likelihood (9) at the end of each filtering run. Figure 5 below shows the likelihood distribution of θ for specific grid point as an example. From this distribution, the mean is chosen as the value for θ to be used in filtering. Different grid points have different geophysical properties and therefore the corresponding physical NPR time series have different properties as well. Therefore the choice of θ depends on the point. However, for simplicity, it was chosen to apply single filtering parameter values globally. The value is chosen from different inspections to be $\theta_0 = 0.003$. For this choice of filtering parameter, likelihood is computed for each grid point. Figure 6 shows an example of model fit map for globally fixed θ_0 .

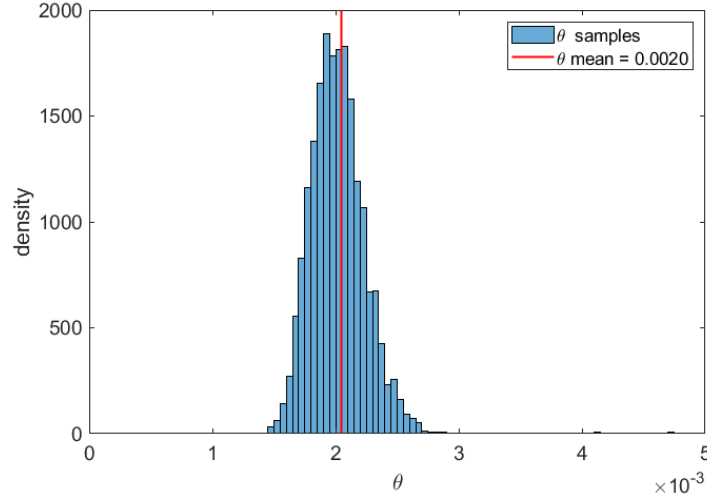


Figure 5: Example of the distribution $p(\theta | r_{1:N}^*, v_{1:N})$ from EASE2.0 grid point centered at 67.3693N, 26.9479E

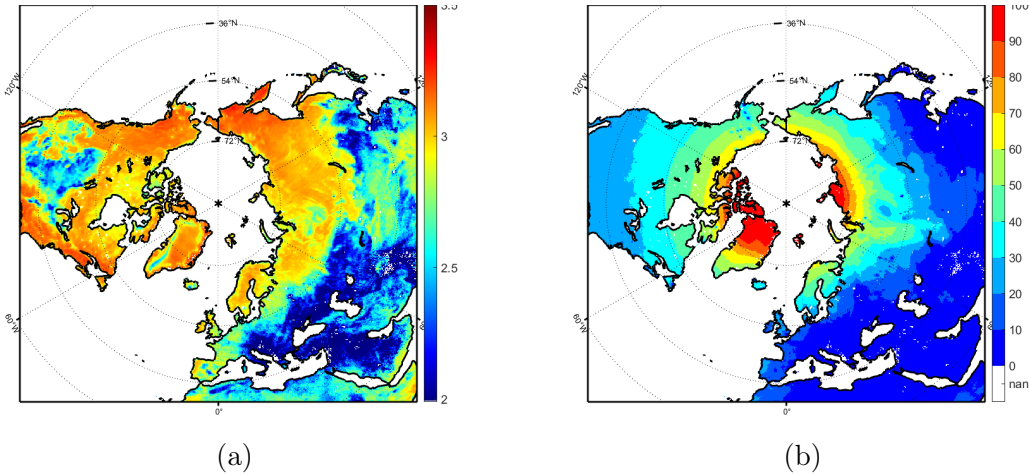


Figure 6: Maps of (a) average model fit $-\frac{1}{N} \log p(\theta | r_{1:N}^*, v_{1:N})$ for global filtering parameter $\theta_0 = 0.003$, (b) average fraction of measurements per day.

3.2.4 Frozen and thaw ground references

The frozen and thaw ground references are generated by the re-processing FT processor when all existing CATDS input data has been processed. The operational FT processor requires pre-defined references to generate the daily FT product.

Scaled NPR value is used to classify the soil freeze-thaw state. To scale the NPR value appropriately, grid point specific frozen (FR) and thaw (TH) soil reference values NPR_{FR} and NPR_{TH} are required. First, the periods when the soil is potentially frozen or thawed are defined. The ancillary input data required for this purpose are ECMWF 2m daily average air temperature data T_{air} and IMS snow cover data. Using the logic shown in Figure 7 each observation is identified as belonging to one of the following categories, (1) potential frozen soil, (2) potential thaw soil, or (3) not defined. A potential frozen soil condition is captured if the air temperature has

been below -3°C and the pixel has a snow cover. A potential thaw soil condition is captured if the air temperature has been above $+3^{\circ}\text{C}$ and there has been over 28 days since the final snow melt-off. The temporal period during which the potential reference observations are searched and identified is from Jan 1st 2014 to Apr 8th 2023. After defining the potential periods representing frozen and thawed conditions, the reference values are determined. For both frozen and thaw soil references NPR_{FR} and NPR_{TH} , the 50 most extreme values are collected and median value is taken for each grid cell to represent frozen and thaw soil references.

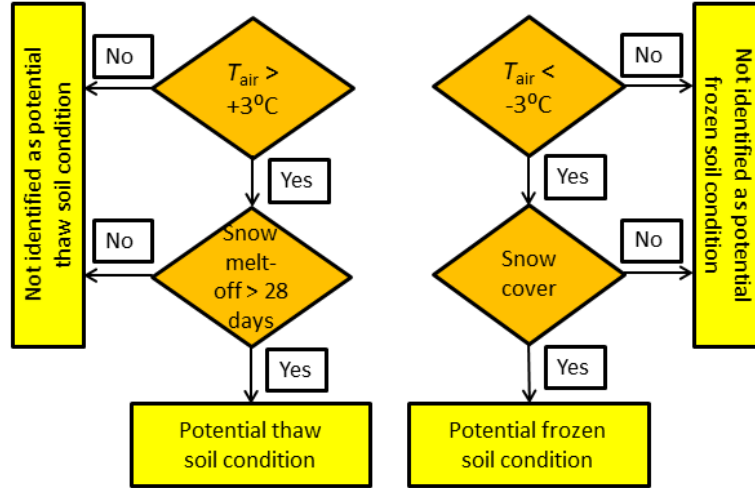


Figure 7: Selection logic for identifying potential thaw and frozen ground observations.

3.2.5 Initial classification and error estimate

The frozen and thaw ground references NPR_{FR} and NPR_{TH} are used to scale the NPR value

$$\text{NPR}_{\text{sca}} = \frac{\text{NPR} - \text{NPR}_{\text{TH}}}{\text{NPR}_{\text{FR}} - \text{NPR}_{\text{TH}}}. \quad (11)$$

An empirical exponential model is used to relate scaled $\text{NPR}_{\text{sca}}(\text{FD})$ with observed frost depth FD

$$\text{NPR}_{\text{sca}}(\text{FD}) = A \cdot (1 - \exp(-B \cdot \text{FD})), \quad (12)$$

where A and B are the fitting parameters. The frost depth observations were acquired from the Finnish Environment Institute (SYKE) network of frost tubes in Finland, selecting only tubes north of the 65 latitude.

Thresholds for soil categorizing are defined as different levels of NPR_{sca} . These thresholds are related to the value of the fitting parameter A . The relation is given in Table 4. The threshold levels in percentages in respect to frozen and thaw soil references are also given in Table 4. Note: $\text{NPR}_{\text{sca}} = 100\%$ corresponds to frozen soil reference and $\text{NPR}_{\text{sca}} = 0\%$ corresponds to thawed soil reference. As the algorithm is partly empirical, its accuracy with respect to in-situ can not be estimated theoretically, but only empirically. However, an error estimate is given which is

soil state category	soil state description	Categorization condition in terms of NPR_{sca} thresholds (%):	Threshold levels in respect to frozen and thaw soil references
1	thaw	$NPR_{sca} < 0.6 \cdot A$	$NPR_{sca} < 50\%$
2	partially frozen	$0.6 \cdot A \leq NPR_{sca} \leq 0.8 \cdot A$	$50\% \leq NPR_{sca} \leq 70\%$
3	frozen	$0.8 \cdot A < NPR_{sca}$	$70\% < NPR_{sca}$

Table 4: Thresholds for the soil state categories in respect to parameter A and in respect to frozen and thaw soil references.

interpreted as precision rather than accuracy. For a fixed grid point, the time series $NPR(t_k)$ is computed by the linear dynamical model (3.2.3) and the Kalman filter algorithm (7). For each time instance t_k

$$NPR(t_k) \sim \mathcal{N}(r_k, u_k^2), \quad (13)$$

where the signal r_k and its uncertainty u_k are estimated by the Kalman filter algorithm (7). Therefore the scaled variable $NPR_{sca}(t_k)$ is also normally distributed for each time step t_k with mean μ_t and standard deviation σ_t given by

$$\begin{cases} \mu_k &= \frac{r_k - NPR_{th}}{NPR_{fr} - NPR_{th}} \\ \sigma_k &= \frac{u_k}{NPR_{fr} - NPR_{th}} \end{cases} \quad (14)$$

The probability of each freeze-thaw category is now computed as the probability of $NPR_{sca}(t_k)$ belonging to corresponding interval, specified in table 4. For example

$$\mathbf{P}(\text{category at time } t_k = \text{frozen}) = \mathbf{P}(NPR_{sca}(t_k) > 0.7) = 1 - F_{\mu_k, \sigma_k}(0.7), \quad (15)$$

where F is the cumulative distribution function of normal distribution with mean μ_k and standard deviation σ_k . This probability reflects the uncertainty of the freeze-thaw state estimate due to the measurement error, but does not reflect the bias and inaccuracy that the algorithm might have due to its empirical components.

3.2.6 Processing mask

The processing mask (PM) is used to regulate the initial classification. PM is a dataset that estimates the expected season for each grid cell on a daily basis. It is generated from the global 2-meter air temperature (T_{air}) and snow cover data.

PM has nine values as listed in Table 5. In order to determine $PM(t)$ for each grid cell for a specific time (day) t , a constant set of criteria were used to define each value of PM. As several changes from a certain value to another were considered to be unlikely, such as a change from summer ($PM(t) = 1$) to the first alarm of spring ($PM(t) = 6$) without intermediate autumn and winter periods ($PM(t) = 2, 3, 4, 5$), the value given for $PM(t)$ was restricted by $PM(t - 1)$ for cases where the previous value was available. The allowed transitions between values from $PM(t)$ to $PM(t + 1)$ are given in Table 5. The criteria for selecting processing mask values for PM (only such values that differ from the previous value) are shown in a block diagram in Figure 8. If no shown criteria is matched, $PM(t)$ equals to $PM(t - 1)$.

PM(t)	Definition	Season	Allowed transitions (PM(t) to PM($t + 1$))
0	undetermined, initial value only	none	1, 3, 5, 7
1	summer	summer	1, 2
2	late summer	summer	1, 2, 3
3	freezing period, early phase	autumn	2, 3, 4
4	freezing period, longer evolved	autumn	3, 4, 5
5	winter	winter	5, 6
6	late winter	winter	5, 6, 7
7	melting period	spring	5, 7, 8
8	end phase of melting period	spring	1, 7, 8

Table 5: The nine values of processing mask PM(t) for time t (day), criteria for their conditions, the respective seasons, and allowed transitions (PM(t) to PM($t + 1$)).

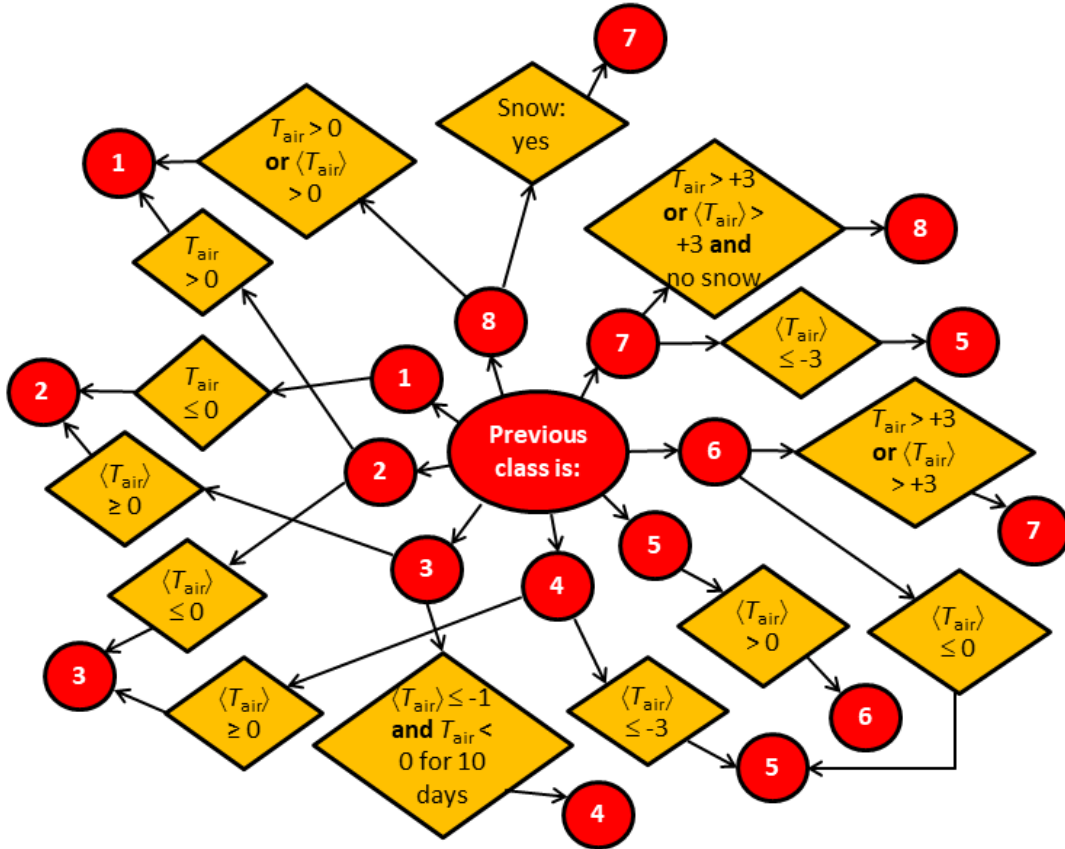


Figure 8: Block diagram of the process on defining the values for PM. Value PM = 0 is only an initial value.

3.2.7 Soil state product generation

The effect of applying the processing mask over the categorized soil F/T-state estimate follows the logic summarized in Table 6. For processing mask values PM(t) = 3 or 4, and 7 or 8 (freezing and melting periods, respectively), the mask has no

effect on the F/T-state estimates. During summer period ($PM(t) = 1$ or 2), all soil F/T-state estimates are forced to the thawed soil state category. During the winter period ($PM(t) = 5$ or 6), the soil state category value is not allowed to decrease; i.e. thawing is not allowed while air temperature T_{air} stays below the selected thresholds shown in Figure 8. No automatic forcing to frozen soil category is applied. It is possible that even during very low temperature conditions, the soil is not frozen due to e.g. thick snow cover that has accumulated prior to sub-zero air temperatures.

$PM(t)$	Effect on to the soil state estimate
1 or 2	forces the soil state to thaw (category 0)
3 or 4	no effect
5 or 6	no effect, if soil state category value increases but soil thawing (i.e. category value decrease) is not allowed
7 or 8	no effect

Table 6: The processing mask levels and their effect on to the final soil F/T-state estimates.

4 References

Helfrich, S., McNamara, D., Ramsay, B., Baldwin, T., and Kasheta, T. (2007). Enhancements to, and forthcoming developments in the Interactive Multisensor Snow and Ice Mapping System (IMS). *Hydrological Processes*, 21, 1576-1586.

Muñoz Sabater, J., (2019): ERA5-Land hourly data from 1981 to present. Copernicus Climate Change Service (C3S) Climate Data Store (CDS), 10.24381/cds.e2161bac

Mätzler C., Ellison, W., Thomas, B., Sihvola, A., and Schwank, M. (2006). Dielectric properties of natural media. In C. Mätzler (Ed.) *Thermal Microwave Radiation: Applications for Remote Sensing* (pp. 427-539). DOI: 10.1049/PBEW052E.

Rautiainen, K., Lemmetyinen, J., Pulliainen, J., Vehviläinen, J., Drusch, M., Kontu, A., et al. (2012). L-Band radiometer observations of soil processes at boreal and sub-arctic environments. *IEEE Transactions on Geoscience and Remote Sensing*, 50(5), 1483–1497

Rautiainen, K., Lemmetyinen, J., Schwank, M., Kontu, A., Menard, C.B., Mätzler, C., et al. (2014) Detection of soil freezing from L-band passive microwave observations. *Remote Sensing of Environment*, 147, 206–218. DOI: 10.1016/j.rse.2014.03.007

Rautiainen, K., Parkkinen, T., Lemmetyinen, J., Schwank, M., Wiesmann, A., Ikonen, J., Derksen, C., Davydov, S., Davydova, A., Boike, J., Langer, M., Drusch, M., Pulliainen, J., (2016) SMOS prototype algorithm for detecting autumn soil freezing. *Remote Sensing of Environment*, SMOS special issue 180:346-360